

Article

Ore Genesis of the Abu Ghalaga Ferro-Ilmenite Ore Associated with Neoproterozoic Massive-Type Gabbros, South-Eastern Desert of Egypt: Evidence from Texture and Mineral Chemistry

Hatem M. El-Desoky¹, Ahmed M. Abdel-Rahman¹, Wael Fahmy¹, Ibrahim Khalifa², Salah A. Mohamed³, Aref Shirazi^{4,*}, Ardeshir Hezarkhani⁴, Adel Shirazy^{4,5} and Amin Beiranvand Pour^{6,*}

¹ Geology Department, Faculty of Science, Al-Azhar University, Cairo 11884, Egypt

² Geology Department, Faculty of Science, Suez Canal University, Ismailia 41522, Egypt

³ Egyptian Mineral Resources Authority (EMRA), 3 Salah Salem St., Abbassia, Cairo 11517, Egypt

⁴ Department of Mining Engineering, Amirkabir University of Technology, Tehran 1591634311, Iran

⁵ Geophysical Institute, Karlsruhe Institute of Technology, 76131 Karlsruhe, Germany

⁶ Institute of Oceanography and Environment (INOS), University Malaysia Terengganu (UMT), Kuala Nerus 21030, Malaysia

* Correspondence: aref.shirazi@aut.ac.ir (A.S.); beiranvand.pour@umt.edu.my (A.B.P.);
Tel.: +98-912-1877608 (A.S.); +60-9-668-3824 (A.B.P.); Fax: +98-21-6640-5846 (A.S.)

Abstract: Massif-type mafic intrusions (gabbro and anorthosite) are known for their considerable resources of vanadium-bearing iron–titanium oxide ores. Massive-type gabbroic and anorthosite rocks are frequently associated with magmatic rocks that have significant quantities of iron, titanium, and vanadium. The most promising intrusions that host Fe-Ti oxide ores are the gabbroic rocks in the south-eastern desert. The ilmenite ore deposits are hosted in arc gabbroic and anorthosite rocks. They are classified into three types, namely black ore, red ore, and disseminated ore. The black ilmenite ore is located at the deeper level, while the oxidized red ore is mainly located at or near the surface. Petrographically, the gabbro and ilmenite ores indicate a crystallization sequence of plagioclase, titaniferous pyroxene, and ilmenite. This reveals that the ilmenite is a magmatic deposit formed by the liquid gravity concentration of ilmenite following the crystallization of feldspar and pyroxene. Meanwhile, quartz, tremolite, zoisite, and opaque minerals are accessory minerals. The Fe-Ti ores are composed of ilmenite hosting exsolved hematite lamellae of variable sizes and shapes, gangue silicate minerals, and some sulfides. The X-ray diffraction (XRD) data reveal the presence of two mineral phases: ilmenite and hematite formed by the unmixing of the ferroilmenite homogeneous phase upon cooling. As a result, the ore is mostly made up of hemo-ilmenite. Using an electron microscope (SEM), as well as by observing the textures seen by the ore microscope, ilmenite is the dominant Fe-Ti oxide and contains voluminous hematite exsolved crystals. Under the scanning electron microscope, ilmenite contained intergrowths of hematite as a thin sandwich and lens shape. The formation of hematite lamellae indicates an oxidation process. Mineral chemistry-based investigations reveal late/post-magmatic activity at high temperatures. The examined ilmenite plots on the ferro-ilmenite line were created by continuous solid solution over 800 °C, whereas the analyzed magnetite and Ti-magnetite plot near the magnetite line and were formed by continuous solid solution exceeding 600 °C.

Keywords: Fe-Ti oxides; Abu Ghalaga district; ilmenite; Fe exsolution; mineral chemistry; gravitational settling; Egypt



Citation: El-Desoky, H.M.; Abdel-Rahman, A.M.; Fahmy, W.; Khalifa, I.; Mohamed, S.A.; Shirazi, A.; Hezarkhani, A.; Shirazy, A.; Pour, A.B. Ore Genesis of the Abu Ghalaga Ferro-Ilmenite Ore Associated with Neoproterozoic Massive-Type Gabbros, South-Eastern Desert of Egypt: Evidence from Texture and Mineral Chemistry. *Minerals* **2023**, *13*, 307. <https://doi.org/10.3390/min13030307>

Academic Editors: Maxim Rudmin and Santanu Banerjee

Received: 13 January 2023

Revised: 16 February 2023

Accepted: 20 February 2023

Published: 22 February 2023



Copyright: © 2023 by the authors. Licensee MDPI, Basel, Switzerland. This article is an open access article distributed under the terms and conditions of the Creative Commons Attribution (CC BY) license (<https://creativecommons.org/licenses/by/4.0/>).

1. Introduction

Mafic intrusions represented by Neoproterozoic anorthosite and gabbroic complexes represent important hosts for global magmatic Fe-Ti oxide ores [1,2]. The Egyptian ilmenite and titaniferous iron ores, with different sources, occur in almost ten locations. They

occur in association with a mafic–ultramafic assemblage having a compositional range of gabbromelanorite to anorthosite. The known occurrences are Homra Dome, Abu Dahr, Wadi Rahabs, Umm Ginud, Wadi El-Miyah, Umm Effein, Korabkanci, Kolmnab, Abu Ghalaga, Umm Tundba, Wadi Yoider, and Gabal Colmenab. The Fe-Ti oxide deposits at Abu Ghalaga and Korabkanci are the two most economically important [3].

Ilmenite (FeTiO_3), hemo-ilmenite (ilmenite with abundant hematite (Fe_2O_3) exsolution lamellae), and titano-magnetite (a solid solution of magnetite ($\text{Fe}^{2+}\text{Fe}^{3+}_2\text{O}_4$) and ulvöspinel (Fe_2TiO_4)) are the most common ore minerals [4,5]. Because Fe-Ti oxide minerals are the most common magnetic particles on Earth, they are essential for paleomagnetic, rock, and environmental applications. The titano-magnetite (TM) and titano-hematite, hemo-ilmenite series are two Fe-Ti oxide solid solution series that are significant for magnetic studies. Anorthosite massifs, charnockite, and (rapakivi) granite are the most common igneous bodies associated with economic magmatic iron–titanium oxide ore deposits [6].

Titanium is found in a concentration of roughly 0.6% in the Earth's crust, making it the fourth most abundant structural metal after aluminum, iron, and magnesium [7]. Approximately 95% of the world's Ti is refined into TiO_2 , a pigment used to create paintings, paper, toothpaste, sunscreen, and plastics with a long-lasting white tint; the remaining 5% is used to produce corrosion-resistant Ti metal [8]. The most common Ti ore types include magmatic deposits with varying quantities of ilmenite, titano-magnetite, and rutile, as well as deposits that have been impacted by secondary metamorphic processes.

Ilmenite is a mineral that can be a major component of Ti ores [9], with a titanium dioxide content of 40 to 65%, ferrous or ferric oxide as the remaining elements, and small amounts of vanadium, magnesium, and/or manganese. Ilmenite represents approximately 92% of global titanium mineral production. Rutile (TiO_2) contains 93–96% titanium dioxide, and it is a widespread mineral in different rock types. The well-known major rutile producers are Australia, South and West Africa, Ukraine, Brazil, etc. Ilmenite is mostly used for its titanium content in the commercial world, whereas iron is largely discarded. Magnetite (Mag) is found in a wide range of magmatic and hydrothermal mineral deposit types, and its wide compositional variability, which is related to the formation environment, has made it a popular tool for mineral deposit prospecting, petrogenesis, and ore genesis.

The Abu Ghalaga ilmenite ore was exploited by the Egyptian ilmenite company until the 1970s. Mining technology is now an open cast above the wadi level [10]. The exploitation stopped due to technical and/or economic circumstances. Discussions regarding the economic future of the ore were carried out in various directions, but no recent studies have been carried out in this context, so this will be the main target of our study.

In our study, we discuss the origin of Fe-Ti ore deposits in the Abu Ghalaga district based on field observations, petrography, ore microscopy, mineralogy (XRD), mineral chemistry, and microchemical analysis using a scanning electron microscope (SEM). The aims of our study can be summarized as follows: (1) to investigate the geological characteristics of ilmenite deposits; (2) to determine the types of ilmenite ore recorded at the Abu Ghalaga mine; (3) to perform a mineralogical and petrographical investigation of Fe-Ti oxides and their host rocks; (4) to study the geochemical behavior of the elements using electron microprobe analyses (EPMA) for Fe-Ti oxides; and (5) to investigate the ore genesis of the Abu Ghalaga ilmenite mine.

2. Geological Setting

According to Figure 1, the Abu Ghalaga area is located in at the south-eastern desert, Egypt, 100 km south of Mersa-Alam City and 17 km west of the Abu Ghosoun port on the Red Sea Coast. It represents a part of the Neoproterozoic Nubian Shield in NE Africa. The study covers approximately 268 km² and is situated between latitudes 24°15'35" and 24°25'35" N and longitudes 35°17'25" and 35°12'01" E.

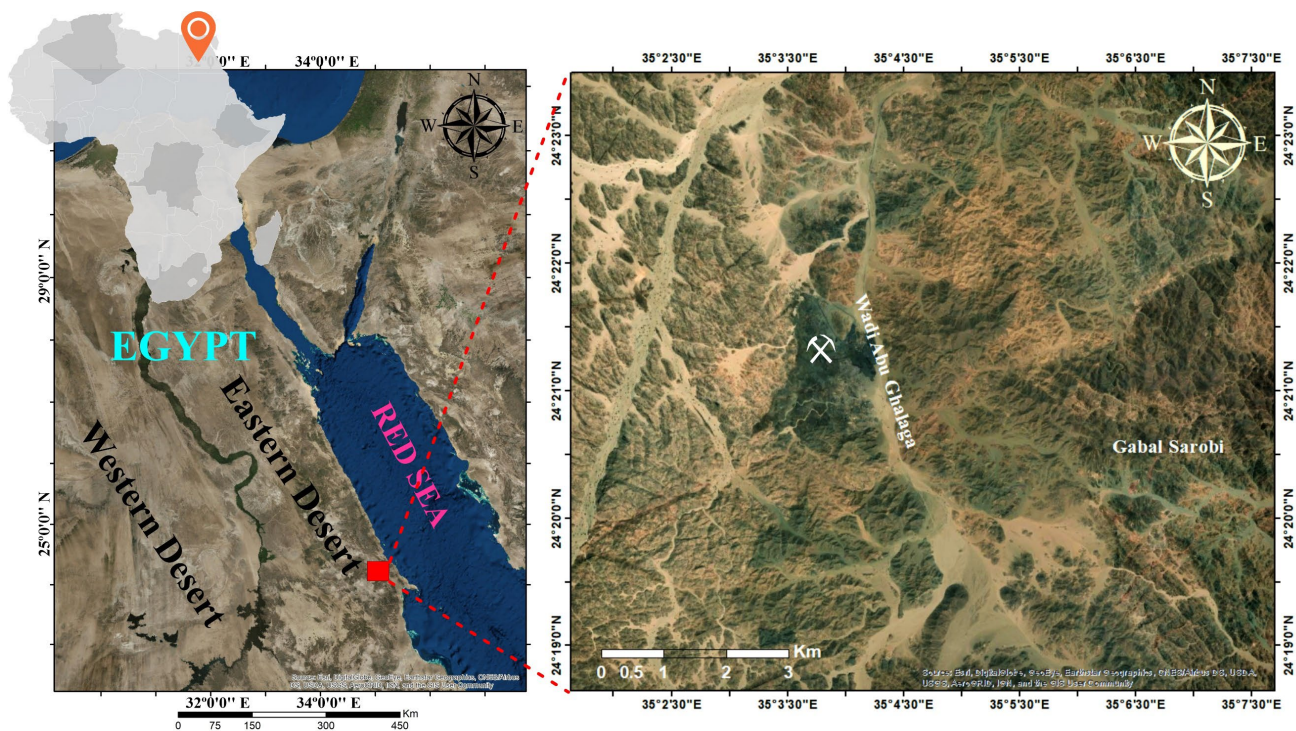


Figure 1. Location map of the Abu Ghalaga district, Egypt, on a Google-based map.

This region (south-eastern desert, Egypt) has been subjected to several regional tectonic movements and magma intrusion, as evidenced by xenolith, particularly the fractures that impacted the gabbroic rocks, allowing ilmenite to disseminate. The present studied area is affected by two principal shear zones [11]: the Nugrus shear zone (NSZ) and the South Hafafit suture (SHS). The Nugrus shear zone (NSZ) is an NW-trending zone of mylonite, schists, and small bodies of gneissic granitoids that runs from the Wadi Nugrus–Wadi Shait junction at the Hafafit complex’s tip to Wadi Abu Ghalaga, a distance of 77 km (Figure 2a,b). The NSZ is represented on most provincial geological maps continuing to the Red Sea Coast at Wadi Ranga, providing an overall length of 85 km [12,13].

The area consists mainly of metavolcanics, gabbroic rocks, and gneissose granites (granodiorite and tonalite), as well as late tectonic intrusions associated with a great deal of mafic to felsic dykes and quartz veins [14]; see Figure 3. The gabbroic rocks are considered as one of the main host rock types of Fe-Ti ore deposits and contain the famous ilmenite ore. The Abu Ghalaga ilmenite ore occurs in the southern part of the Abu Ghalaga gabbroic intrusion cropping out along the western bank of Wadi Abu Ghalaga (Figure 3). The Abu Ghalaga mine has the largest Fe-Ti ore reserve in Egypt [15,16]. Vanadium is one of the important elements associated with the Fe-Ti ore, and it was recorded in some analyses from 0.29 to 0.79 wt.% [3,17,18]. The main V carriers in these deposits are generally titanium-rich magnetite and ulvöspinel and ilmenite [18].

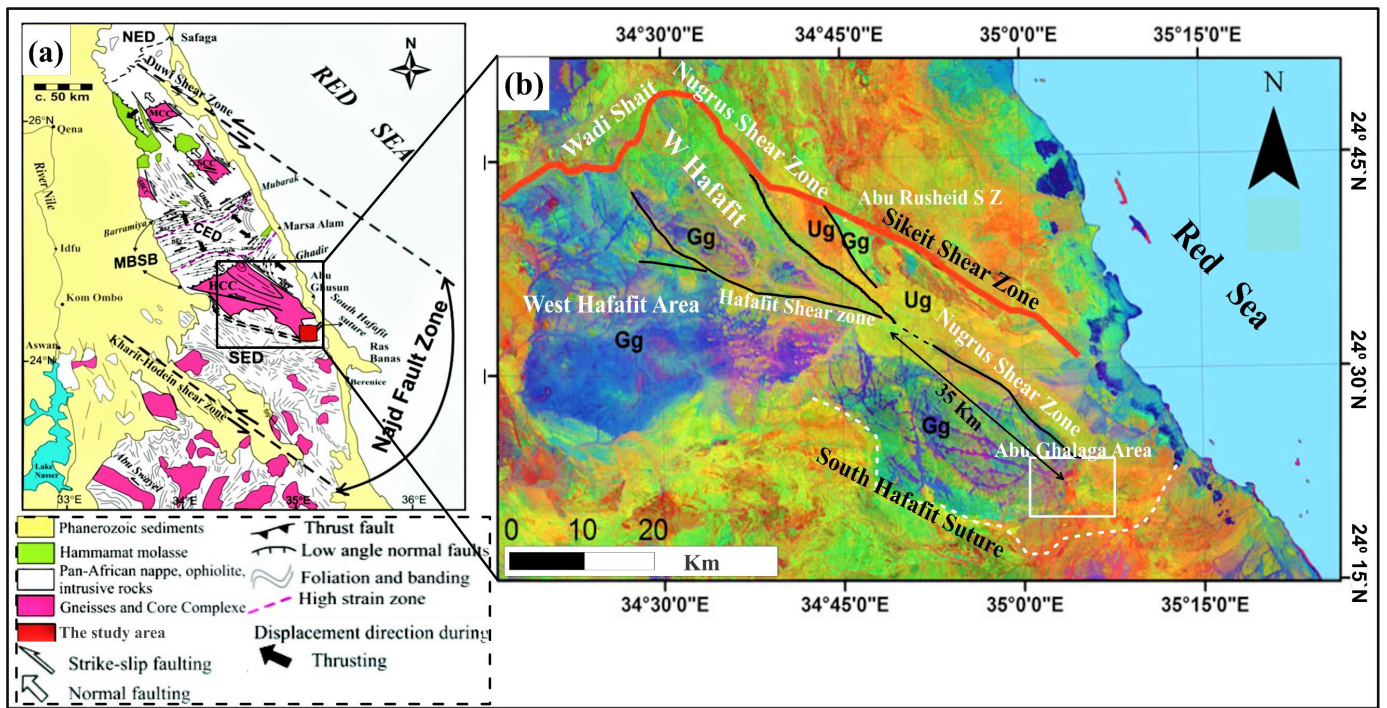


Figure 2. (a) Major structures in the central eastern desert (CED) and south-eastern desert (SED). Abbreviations: NED—north-eastern desert, NSZ—Nugrus shear zone, UNSZ—Um Nar shear zone, HCC—Hafait core complex, SCC—Sibai core complex, MCC—Meatiq core complex, MBSB—Mubarak-Baramiya shear belt, Gg—granitoid gneisses, and Ug—undifferentiated gneisses. This map is compiled from [19,20]. (b) False color principal component image of Landsat 8 satellite image (PC5, PC4, PC2 in RGB) for Abu Ghalaga area affected by the Nugrus shear zone and South Hafait suture after [13]. NSZ is NW-oriented, extending for approximately 77 km in the SED of Egypt.

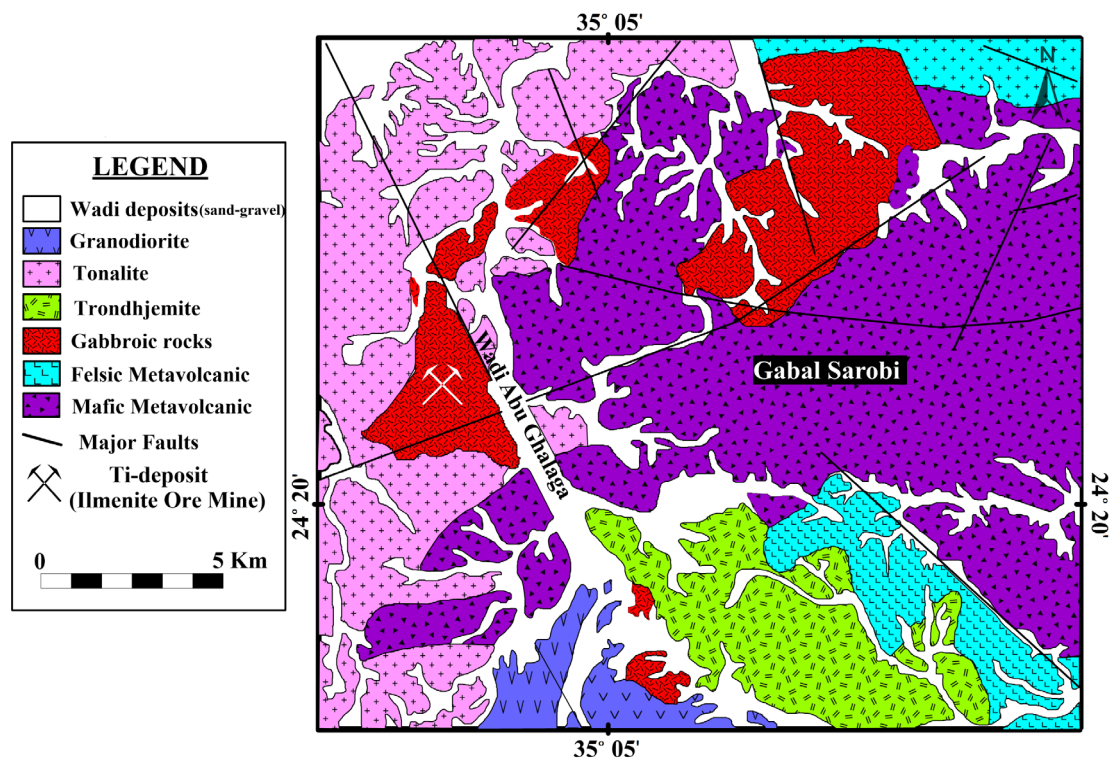


Figure 3. Geological map of Abu Ghalaga area, modified after [21,22].

The gabbroic rocks are generally medium-grained and are frequently banded. They commonly enclose irregular inclusions and narrow dykes of coarse-grained gabbro, as well as occasional small lenses of fine-grained gabbro. The pegmatite gabbro is highly altered, probably as a result of autometasomatism and the concentration of volatiles during the late stages of crystallization of the magma. The gabbroic rocks display a well-developed primary banding, shown as segregation banding on a cm scale of medium- to coarse-grained pyroxene + hornblende-rich bands alternating with plagioclase bands and ilmenite-rich bands.

The ilmenite ores occur as lenses and sheet-like bodies that follow NW-SE and SE patterns and dip 30° to the NE. It is hosted in the gabbro complex located in the central part of the Abu Ghalaga area (Figure 4a,b). Its thickness is around 30 m and its length is around 300 m, revealing dark blackish-grey altered bands and massive pockets.

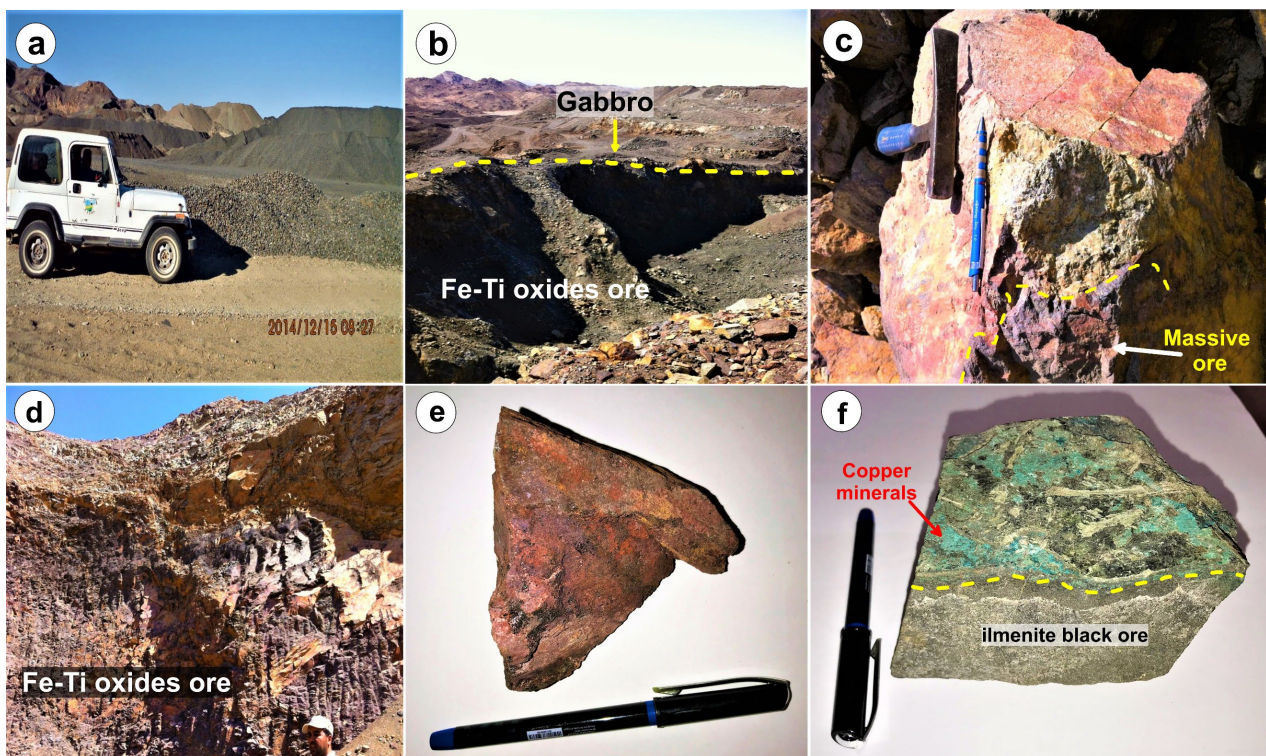


Figure 4. Field relationships between the Fe-Ti oxides bodies and their host rocks. (a) Abu Ghalaga mine. (b) Black (fresh) ore and red (oxidized) ore hosted in the gabbroic rocks. (c) Massive ore. (d) and (e) Black (fresh) ore and red (oxidized) ore. (f) Green copper mineral staining along the boundaries of ilmenite ore.

Three types of ilmenite ore are recorded at the Abu Ghalaga mine: (a) a cap or surface ore, (b) a red ore or oxidized zone, and (c) a black ore or the main body (fresh) ore [23]. The cap ore forms a surface crust, covers the top of the main ilmenite body, and does not exceed 50 cm in thickness. The ore is usually friable as a result of having been subjected to extensive weathering (Figure 4d). The red ore occurs immediately below the cap ore, forming a thick, red, oxidized coating outside the main ilmenite mass, which may reach several meters in thickness (Figure 4e). This type represents the oxidized ore, the reddish-brown color of which is due to the partial alteration of ilmenite to hematite, goethite, and limonite. It is usually friable, but occasionally very hard and massive, and is generally highly fractured and jointed. The black ore forms the main part of the ilmenite deposit. Its typical forms are hard, massive, and fine-grained with a submetallic luster and are usually black in color (Figure 4c). The greenish color of copper carbonate forms a thin band along

the borders of the black ilmenite mass and its upper parts (Figure 4e) and it is somewhat common to the northwest of the main ilmenite lens.

3. Materials and Methods

Twenty rock samples, from the Abu Ghalaga gabbroic complex, were collected. The field study was focused on the open cast area of the Abu Ghalaga mine, where ilmenite is exposed in the central part of the studied district. Twelve thin sections of gabbro were microscopically studied by a polarizing microscope to display the mineral composition, microstructures, textures, and alteration types of the studied rocks. Eleven polished sections were prepared to identify the opaque minerals, as well as their intergrowth and replacement textures. Eleven samples of the iron–titanium oxides were examined using an X-ray diffractometer (XRD) at the Central Laboratories of the Egyptian Mineral Resources Authority, Cairo, Egypt. X-ray diffraction (XRD) patterns were recorded on Philips Pw 1710 X-ray diffraction equipment with a monochromator; Cu radiation ($\lambda = 1.542$ nm) at 50 kV, 40 mA, and scanning speed $0.02^\circ/\text{s}$. were used. The Fe-Ti ore samples were investigated under scanning electron microscopy–energy-dispersive X-ray (SEM-EDX) microchemical analysis at the Egyptian Mineral Resources Authority, Central Laboratories Sector, Egypt, using the SEM Model Quanta 250 Field Emission Gun (FEG) attached to an EDX Unit (Energy-Dispersive X-Ray Analyses), with accelerating voltage 30 kV, magnification $14\times$ up to $1,000,000\times$, and resolution for the gun of 1n. Operating conditions were as follows: 20 kV accelerating potential using ZAF correction factors. Quantitative chemical analyses of ore minerals were carried out using electron probe micro-analyzer (EPMA) analysis (accuracy of 1–2% for major elements and varied from 2 to 20% for trace elements) at Wurzberg University, Wurzberg, Germany. Table 1 shows the sampling details, such as the types and numbers, as well as the analysis methods used.

Table 1. The number and type of samples collected, as well as the analysis methods used.

Type of Samples	Number of Samples	Methods of Analysis
Hand specimens of gabbro and Fe-Ti oxides	52	
Thin section of gabbro (petrography)	12	Polarizing microscope.
Thin polished sections (mineralogy)	11	Reflected light microscope.
Fe-Ti ore samples	11	X-ray diffractometer (XRD)
Mineral chemistry analyses of Fe-Ti ore	38	Scanning electron microscope (SEM-EDX)
		Electron microprobe analysis (EPMA)

4. Results and Analysis

4.1. Petrography of Gabbros

The gabbroic rocks that are exposed in the central part of the region are coarse-to-medium-grained, composed of altered plagioclase, clinopyroxene, and hornblende. Alteration products include saussurite, epidotization, and carbonization. Quartz, tremolite, zoisite, and opaque minerals are the main accessory minerals.

Plagioclase is calcic-type (andesine to labradorite: An₄₀-An₆₀); it occurs as strongly altered (saussuritized) tabular hypidiomorphic crystals. They exhibit a Carlsbad and percline twinning (Figure 5a). Fine-grained plagioclase crystals are recorded enclosed partly and sometimes completely in the pyroxene (Figure 5a). Pyroxene occurs as highly altered hypidiomorphic augite crystals. The prismatic clinopyroxene crystals are partially and completely altered to tremolite–actinolite and hornblende (Figure 5b,c). The crystals are sometimes invaded by carbonate minerals. Hornblende occurs as brownish, hypidiomorphic to allotriomorphic crystals showing strong pleochroism (Figure 5d). Tremolite occurs as idiomorphic to xenomorphic crystals, of pale brown color, showing weak pleochroism. They appear along prismatic crystals resulting from the alteration products of pyroxene (Figure 5b). Opaques are represented by fine-grained to coarse aggregates that occur as interstitial phases and are scattered throughout rock crystals (Figure 5e,f).

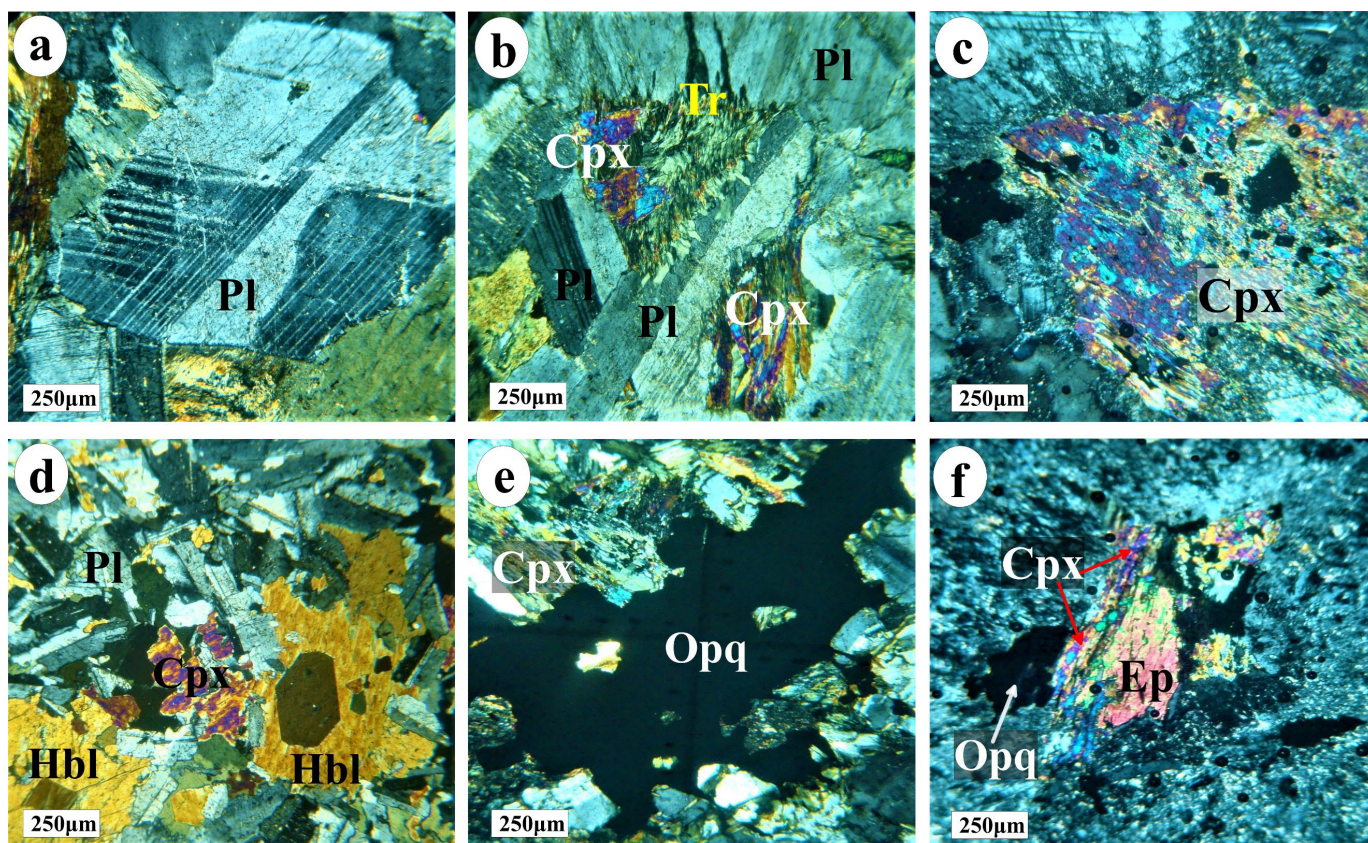


Figure 5. Petrographic characteristics under cross-polarized (XPL) analysis of Abu Ghalaga. (a) Percline twinning of plagioclase (Pl). (b) Sub-ophitic texture showing clinopyroxene (Cpx) altered to tremolite (Tr) and Carlsbad twinning of plagioclase (Pl). (c) Well-developed crystal of clinopyroxene (Cpx) with small spot of opaque minerals (Opq). (d) Hornblende (Hb) after clinopyroxene (Cpx). (e) Fe-Ti oxide (Opq=magnetite/ilmenite) occurs as interstitial mineral between silicate minerals. (f) Epidote (Ep) is the alteration product after clinopyroxene (Cpx).

4.2. Mineralogy and Petrography of Fe-Ti Oxides

The most frequent opaque minerals found in gabbro are ilmenite and hematite. Ilmenite is light greyish-white in color and exhibits moderate reflectance. It contains fine-to medium-grained, anhedral-to-euhedral crystals dispensed throughout the host rock (Figure 6a) [24]. Ilmenite grains are constantly twin-lamellated to a high degree. Ilmenite (grey) with hematite (white) exsolution was recorded in two generations. Very fine exsolution of magnetite and rutile can be noticed as small, extended particles standing at right angles to the basal discs. Hematite fills the cracks and the interspaces between crystals and along the fractures of the ilmenite (Figure 6b,c).

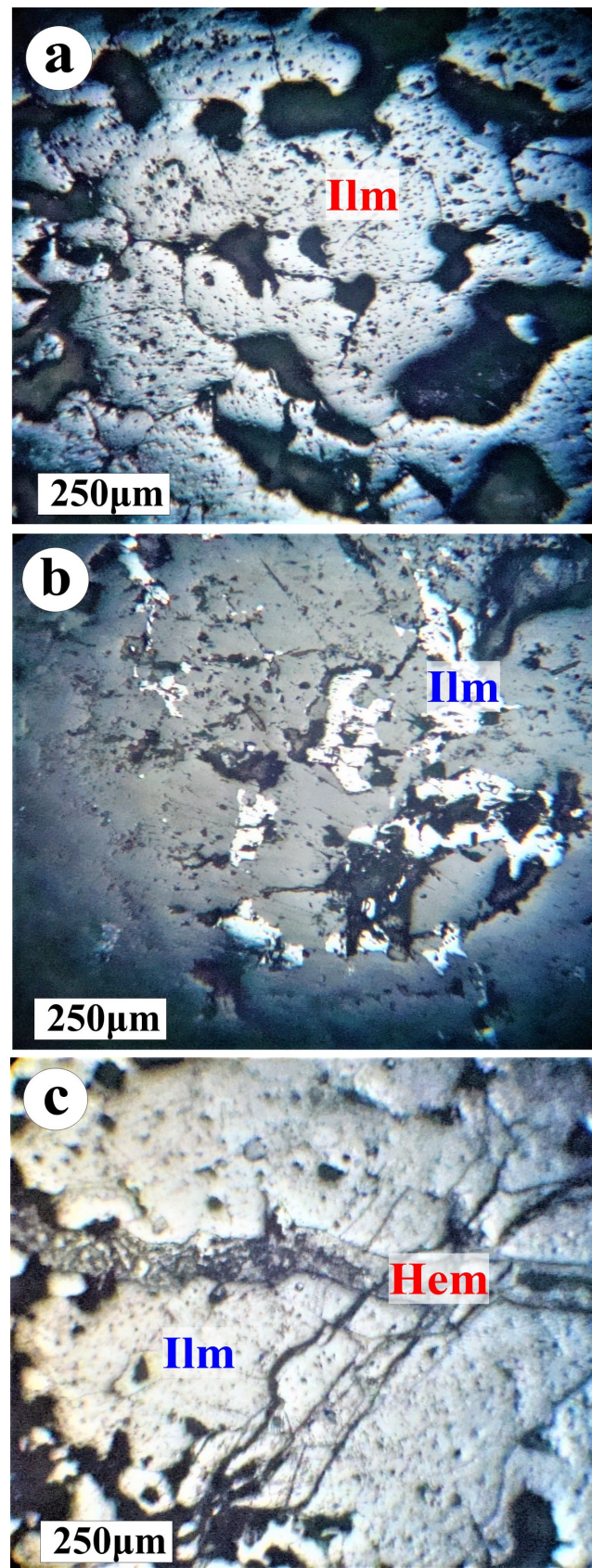


Figure 6. Polished section of an ilmenite crystal showing (a) reflected light photomicrographs, showing rounded fine-grained ilmenite (Ilm); (b) isolated ilmenite (Ilm) in gabbro; (c) hematite (Hem) cutting ilmenite (Ilm) crystals.

4.3. Microchemical Analysis by Scanning Electron Microscope (SEM-EDX)

The opaque (Fe-Ti oxides) minerals are represented by ilmenite and hematite (Figure 7a–d). Two types of textures are shown by the mineralogical and textural study: thin sandwich lamellae (Figure 7a) and lens shapes (Figures 6c and 7b). The occurrence of a sandwich intergrowth indicates that the oxidation has started at a high temperature. One of the most common types of hematite in the ilmenite exsolution of gabbro is represented by thin lamellae. The network density falls as the Ti content drops, and the hematite eventually becomes uniform, containing only one or two very thin ilmenite lamellae on rare occasions (Figure 7d).

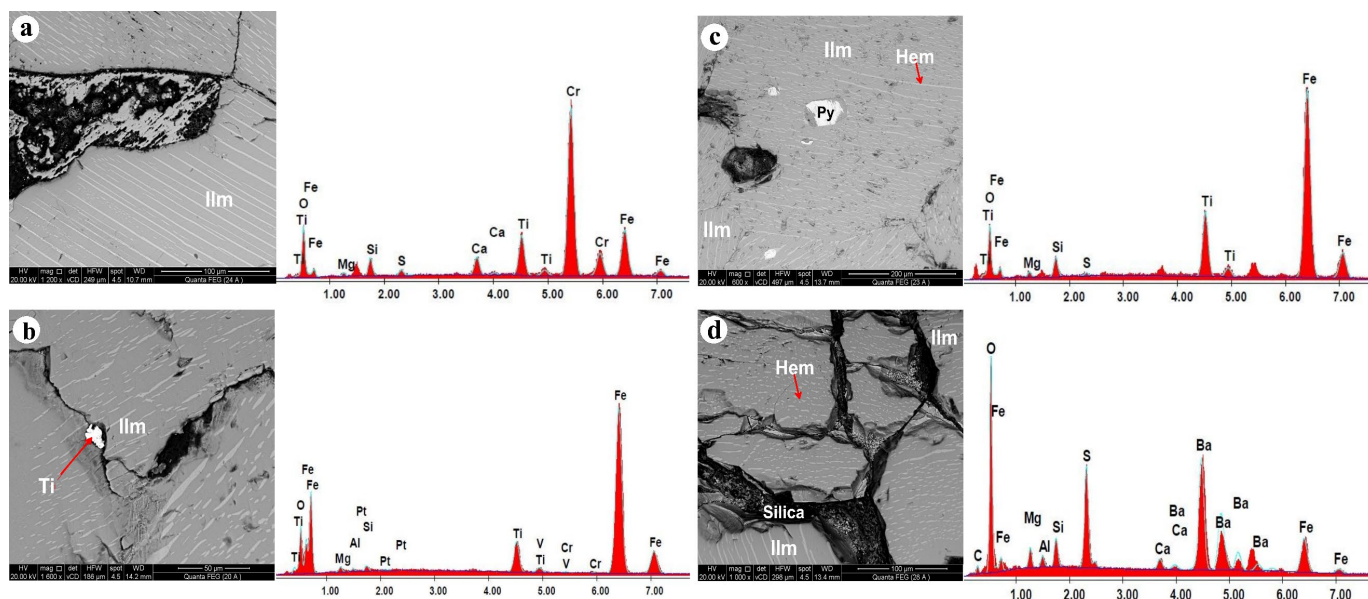


Figure 7. Back-scattered electron (BSE) images and EDX spot analyses of the studied Fe-Ti oxides. (a) Exsolution of intergrowth of ilmenite sandwich. (b) Lens-shaped exsolution of hematite in planes of the host ilmenite. (c) Ilmenite with very fine hematite exsolution lamellae associated with pyrite crystal (Py). (d) Hemo-ilmenite demonstrated by a progressive increase in size and number of hematite lenses and silicate content along fracture.

According to [25,26], the detailed formula of ilmenite is $(\text{Fe}, \text{Mg}, \text{Mn})\text{TiO}_3$ with a restricted quantity of Mg^{+2} and Mn^{+2} , which substitutes the Fe^{+2} in the original ilmenite lattice, as well as the current findings [27]. During chemical weathering, other elements such as Al, Si, Th, P, V, and Cr are typically absorbed into ilmenite grains. Ca, Mn, and Al form part of the crystal structure of ilmenite, present as impurities within and between each other, and result in the contamination of the host rocks. Because most Ni acts as a compatible element in igneous differentiation processes and minor levels of nickel sulfides are present in mantle peridotites, the development of nickel-bearing sulfides is practically limited to sulfide-overloaded mafic and ultramafic melts. Furthermore, the presence of a high peak of barite crystals is considered to indicate the contamination of the hosted gabbroic rocks.

4.4. X-ray Diffraction Analysis (XRD)

The mineralogical composition of the twelve ore samples defined by X-ray diffraction (XRD) is illustrated in Figure 8. Ilmenite and hematite are the essential ore minerals in the studied district. Meanwhile, the gangue minerals are chlorite, anorthite, clinocllore, actinolite, calcite, dolomite, kaolinite, and protomangano-ferroanthophyllite (Table 2 and Figure 8). Several gangue minerals are also observed with the hemo-ilmenite of Abu Ghalaga. The principal gangue minerals in the gabbroic rocks with magmatic Fe-Ti oxide deposits are plagioclase ($\text{An}_{40}\text{--}\text{An}_{60}$), clinopyroxene, hornblende, tremolite, chlorite,

Table 2. Identified mineral phases in Fe-Ti oxides.

	Mineral and Abbreviation	Formula	Relative Content
1	Ilmenite (Ilm)	FeTiO ₃	20–85%
2	Hematite (Hem)	Fe ₂ O ₃	13–77%
3	Chlorite (Chl)	Fe, Mg, Al) ₆ (Si, Al) ₄ O ₁₀ (OH) ₈	4–14%
4	Anorthite (An)	CaAl ₂ Si ₂ O ₈	6%
5	Chlinochlore	Mg ₅ Al(AlSi ₃ O ₁₀)(OH) ₈	5–20%
6	Actinolite (Act)	Ca(Mg _{4.5-2.5} Fe _{0.5-2.5})Si ₈ O ₂₂ OH ₂	2–21%
7	Calcite (Cal)	CaCO ₃	1%
8	Dolomite (Dol)	CaMg(CO ₃) ₂	3%
9	Kaolinite (Kln)	Al ₂ Si ₂ O ₅ (OH) ₄	2–10%
10	Hornblende (Hbl)	(Ca,Na) ₂ (Mg,Fe,Al) ₅ (Al,Si) ₈ O ₂₂ (OH) ₂	15%
11	Anthophyllite (Ath)	(Mg, Fe ²⁺) ₇ Si ₈ O ₂₂ (OH) ₂	3%

Note: Abbreviations for names of rock-forming minerals [28].

4.5. Chemical Composition of the Fe-Ti Oxides

Electron probe analytical data obtained for several of the Fe-Ti oxide minerals of the Abu Ghalaga ores are given in Tables 3 and 4 and are represented in Figure 9. The investigated Fe-Ti oxides from the gabbros in the Abu Ghalaga area can be classified as ilmenite and titanomagnetite based on their chemical properties. The characteristics of the analyzed minerals are summarized in the following.

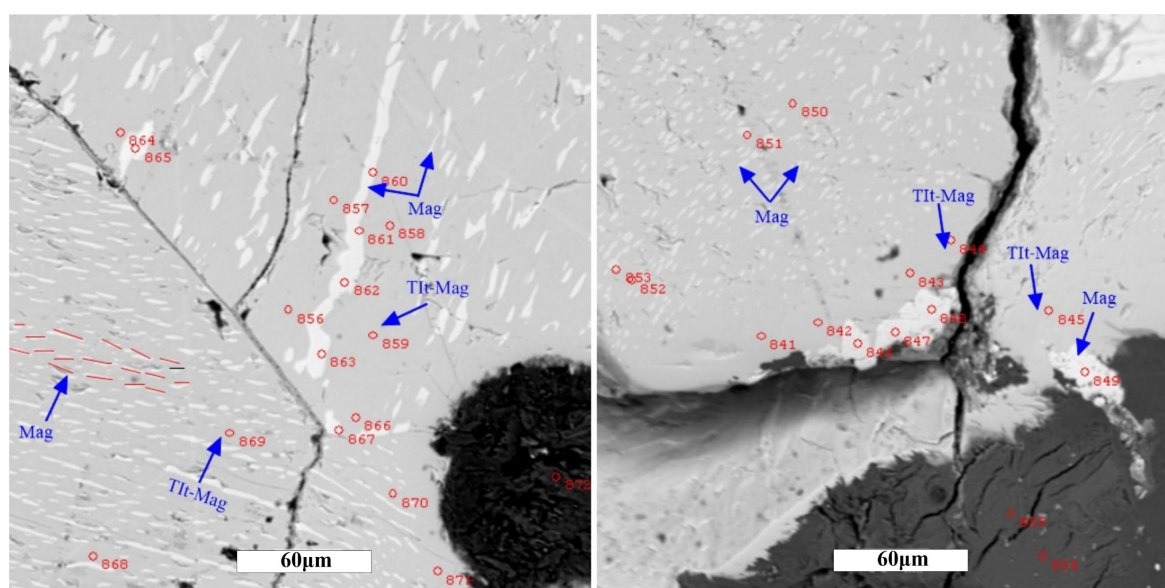


Figure 9. Back-scattered electron (BSE) images of iron titanium oxide intergrowth.

The analyzed ilmenite minerals of the Abu Ghalaga area nearly approach the ideal composition, with TiO₂ ranging between 44.51 and 49.07% (average 48.11%), and FeO^t between 48 and 52.43% (average 49.51 wt.%). In addition, they have a small amount of MgO (0.87 to 1.9%), MnO (0.22–0.35 wt.%), Cr₂O₃ (0.00–0.6 wt.%), Na₂O (0.00–0.05 wt.%), CaO (0.00–0.05 wt.%), and Al₂O₃ (0.00–0.26 wt.%) and trace amounts of SiO₂ and ZnO.

The titanomagnetite minerals of the Abu Ghalaga area contain FeO^t ranging between 76.38 and 88.59% (average 83.0%), and TiO₂ between 1.38 and 18.52% (av. 8.88%). They have a small amount of MgO (0.01 to 0.27%), MnO (0.00–0.05 wt.%), Cr₂O₃ (0.30–0.67 wt.%), Na₂O (0.00–0.05 wt.%), CaO (0.00–0.06 wt.%), and Al₂O₃ (0.01–0.35 wt.%) and trace amounts of SiO₂ (0.00–0.79 wt.%) and ZnO (0.0–0.26%). In comparison to ilmenite, the titanomagnetite has high FeO content and a very low TiO₂ level (Table 4).

Table 3. Representative electron microprobe analyses of ilmenite from the Abu Ghalaga mine, Egypt.

Sample (%)	Un 99 6 ROI1						Un 100 6 ROI2						
	829	830	831	832	833	838	841	842	843	844	845	850	851
SiO ₂	0.008					0.026				0.018			
TiO ₂	47.97	48.81	48.23	48.8	48.4	48.64	48.46	48.45	47.95	47.94	48.98	45.4	44.51
Al ₂ O ₃				0.02			0.02	0.01	0.05	0.01			0.26
FeO ^t	48.94	48.85	49.15	48.77	48.91	49.32	49.65	49.89	50.28	50.59	49.72	51.76	52.43
MgO	1.642	1.707	1.628	1.678	1.823	1.67	0.93	0.919	0.884	0.873	0.781	1.055	1.007
Cr ₂ O ₃	0.02	0.06	0.03	0.01	0.02	0.03	0	0.02	0.01	0.05	0.03	0.06	0.05
MnO	0.29	0.3	0.26	0.34	0.29	0.34	0.32	0.29	0.34	0.28	0.32	0.33	0.22
NiO									0.021				
ZnO		0.04	0.32	0.008			0.23		0.04	0.22	0.31	0.008	
Total	98.92	99.77	99.63	99.65	99.46	100	99.6	99.6	99.6	100	100.2	98.7	98.5
Structural formula is based on 6 oxygen atoms													
Si	0.28	0.29	0.29	0.29	0.29	0.29	0.29	0.29	0.28	0.28	0.29	0.28	0.28
Ti	1.67	1.69	1.68	1.69	1.68	1.68	1.69	1.69	1.67	1.67	1.7	1.59	1.56
Al				0.001			0.001	0.001	0.003	0.001			0.01
Fe ²⁺	1.9	1.88	1.89	1.88	1.88	1.89	1.93	1.93	1.95	1.96	1.92	2.02	2.05
Mg	0.11	0.11	0.11	0.11	0.12	0.11	0.06	0.06	0.06	0.06	0.05	0.07	0.07
Cr	0.001	0.002	0.001		0.001	0.001		0.001		0.002	0.001	0.002	0.002
Mn	0.01	0.01	0.01	0.01	0.01	0.01	0.01	0.01	0.01	0.01	0.01	0.01	0.009
Ni								0.29	0.28	0.28	0.29		
Zn			0.005				0.004	1.69	1.67	1.67	1.7		

Sample (%)	Un 100 6 ROI2					Un 99 6 ROI3						
	852	853	856	857	858	859	864	866	868	869	870	871
SiO ₂												
TiO ₂	49.07	46.77	48.9	48.3	48.8	47.9	47.6	48.7	48.2	48.1	49	48.9
Al ₂ O ₃	0	0.02	0	0	0	0	0	0	0	0	0	0
FeO ^t	48.99	51.1	48.8	49.4	49.1	49.8	48.9	49	48.8	49.2	48	48.5
MgO	1.01	0.95	1.82	1.83	1.86	1.76	1.8	1.88	1.79	1.76	1.9	1.78
CaO	0.05	0.01				0.01		0.01	0	0	0	0.02
Na ₂ O	0.01		0.02		0.01		0.03				0.03	0.01
K ₂ O												0.01
Cr ₂ O ₃	0.01	0.02	0.01	0.03	0.01	0.02	0.05	0.01	0.04	0.04	0.01	0.01
MnO	0.29	0.31	0.25	0.31	0.26	0.26	0.32	0.25	0.32	0.28	0.29	0.3
NiO												
ZnO	0.04	0.3	0.16		0.44		0.2			0.02		
Total	99.5	99.5	100	99.9	100.6	99.8	99	99.8	99.2	99.4	99.2	99.6
Cation ratios based on O = 6												
Si	0.29	0.28	0.29	0.28	0.29	0.28	0.28	0.29	0.29	0.28	0.29	0.29
Ti	1.71	1.64	1.69	1.67	1.68	1.66	1.66	1.68	1.68	1.67	1.7	1.69
Al		0.001	0.001		0.001							
Fe ²⁺	1.9	1.99	1.877	1.9	1.88	1.91	1.9	1.88	1.89	1.9	1.85	1.87
Mg	0.07	0.06	0.125	0.12	0.12	0.12	0.12	0.12	0.12	0.12	0.13	0.12
Cr		0.001		0.001		0.001	0.002		0.002	0.002	0	0.001
Mn	0.01	0.01	0.01	0.01		0.01	0.013		0.01	0.01	0.01	0.01
Zn			0.003		0.007		0.003					

The plotted samples on the TiO₂-FeO-Fe₂O₃ ternary diagram [29] reveal that the studied Fe-Ti oxides are related to ilmenite-hematite series and ulvöspinel-magnetite series (Figure 10). The Fe-Ti oxide minerals from gabbroic rocks exhibit a significant negative correlation of TiO₂, MnO, and Al₂O₃ with FeO, while it shows a positive correlation with Cr₂O₃ (Figure 11). Iron-titanium oxides represented by magnetite, and hematite exsolutions

occur as irregular aggregates (Figure 12). Rutile forms an intergrowth as a secondary phase by oxidation, most probably as post-ore formation.

Table 4. Representative electron microprobe analyses of titano-magnetite from the Abu Ghalaga mine, Egypt (all values are in wt.%).

Samples(%)	Titano-Magnetite				Ti-Poor Magnetite				Titano-Magnetite				
	834	835	836	837	846	847	848	849	861	862	863	865	867
SiO ₂					0.472	0.354	0.48	0.78					
TiO ₂	11.57	12.45	12.56	18.52	1.38	1.96	1.57	1.66	11.3	12.5	11.4	7.5	11.1
Al ₂ O ₃	0.04	0.06	0.01	0.06	0.17	0.20	0.14	0.35	0.1	0.2	0.1	0.1	0.1
FeO	80.95	80.41	80.74	76.38	88.13	88.57	88.59	86.99	80.6	79.6	81.2	85.6	81.3
Fe ₂ O ₃	6.86	6.49	6.06	4.46	9.43	8.41	8.86	10.26	7.48	6.95	6.67	6.36	6.96
MgO	0.15	0.22	0.24	0.18	0.02	0.008	0.02	0.06	0.17	0.27	0.18	0.07	0.15
CaO	0.01	0.01	0.01		0.04	0.03	0.04	0.06					
Na ₂ O	0.05	0.01		0.05		0.02	0.03	0.03			0.01		
K ₂ O					0.002		0.003						
Cr ₂ O ₃	0.33	0.33	0.33	0.30	0.67	0.54	0.53	0.58	0.35	0.36	0.41	0.32	0.37
MnO	0.03	0.01	0.04	0.04			0.02			0.01	0.03	0.04	0.02
NiO												0.01	
ZnO					0.14	0.25	0.18			0.11			
Total	100	100	100	100	100	100	100	100	100	100	100	100	100
Cation ratios based on O = 6													
Si	0.22	0.22	0.22	0.23	0.21	0.21	0.20	0.21	0.24	0.22	0.22	0.21	0.22
Ti	0.42	0.45	0.45	0.66	0.05	0.07	0.01	0.06	0.72	0.41	0.46	0.27	0.41
Al	0.003	0.003	0.001	0.003	0.01	0.01	0.02	0.02	0.002	0.005	0.01	0.003	0.005
Fe ²⁺	3.31	3.28	3.28	3.06	3.69	3.67	3.71	3.66	2.96	3.32	3.26	3.48	3.33
Mg	0.01	0.01	0.01	0.01	0.002	0.001	0.002	0.005	0.04	0.01	0.02	0.005	0.01
Cr	0.01	0.01	0.01	0.01	0.02	0.02	0.02	0.02					
Mn	0.001	0.001	0.002	0.002					11.3	12.5	11.4	7.5	11.1
Ni									0.1	0.2	0.1	0.1	0.1
Zn					0.003	0.005			80.6	79.6	81.2	85.6	81.3

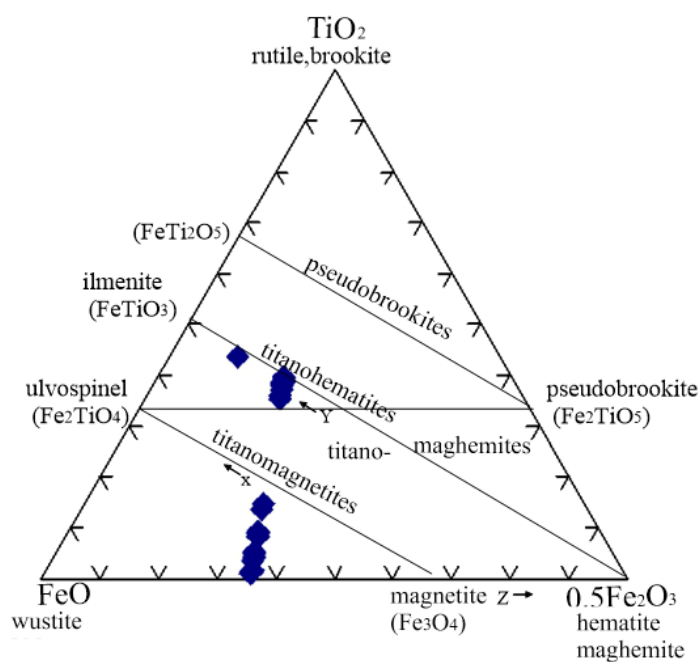


Figure 10. Ternary system of TiO₂-FeO-1/2Fe₂O₃ [30] showing the titano-magnetite and titanohematite-hemoilmenite solid-solution lines and the titano-maghemite composition.

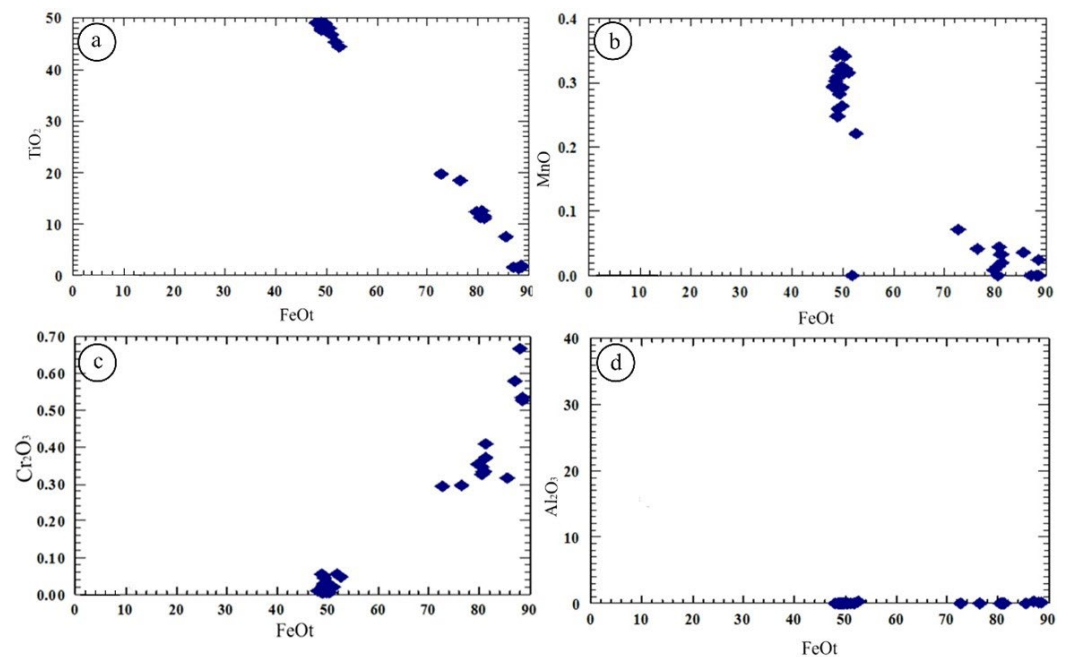


Figure 11. Binary plots of concentrations of wt.% of some elements versus FeO^t for ilmenite and titanomagnetite in the Abu Ghalaga gabbro intrusion. (a) TiO₂; (b) MnO; (c) Cr₂O₃; (d) Al₂O₃.

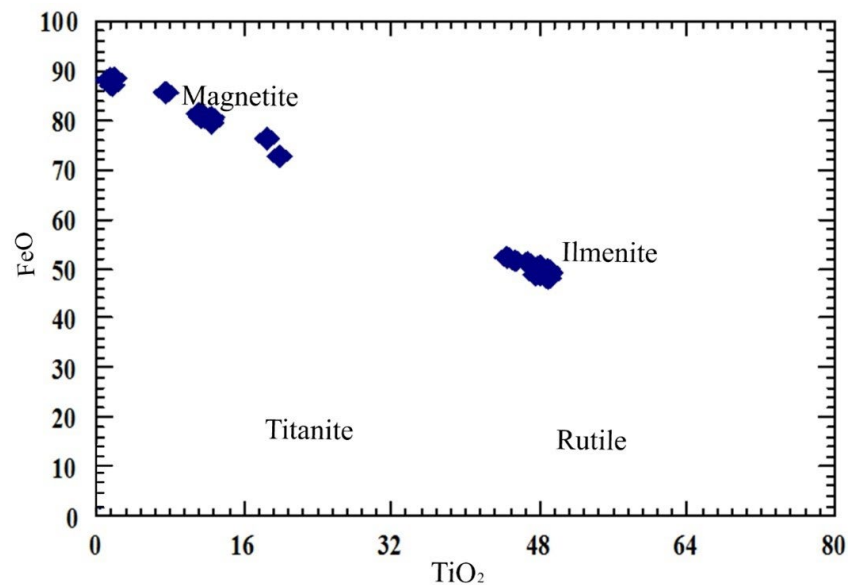


Figure 12. FeO (wt.%) versus TiO₂ (wt.%) variation diagram showing the chemical constituents of the studied minerals [24].

5. Discussion

5.1. Formation of Fe-Ti Oxide Ore

Two factors explain the origin of the Fe-Ti oxide ores in the gabbroic rocks: the first one is a magmatic origin, in which many researchers suggest that this process is related to the gravity setting of Ti-magnetite and ilmenite [31]. In this respect, the primary oxide was aluminous Ti-magnetite (Usp40) with 40 wt.% FeO, 34 wt.% Fe₂O₃, 16.5 wt.% TiO₂, 5.3 wt.% Al₂O₃, 3.5 wt.% MgO, and 0.5 wt.% MnO, which corresponds to the bulk ore composition [32]. The other possibility supposes that the ore formation was related to the exsolution of Fe-rich liquid [33]. This idea is based on recent experiments [34], which demonstrate the possibility of the immiscible splitting of an evolved ferrobaltic magma into Fe-Ti-(P)-rich and silicate-rich liquids; an Fe-rich melt is much lower-temperature

compared to a pure Fe-Ti oxide melt. Hematite can be generated either through the transformation of previously formed magnetite or directly by intracrystalline Fe^{2+} ion migration. All the analyzed Fe-Ti oxides contain small amounts of Cr_2O_3 , suggesting its crystallization from an already evolved melt [33].

The Ti oxide phases, ilmenite, and rutile, which are stable under upper mantle conditions, exhibit phase transformations to higher-pressure polymorphs. TiO_2 is stable as rutile under low-pressure conditions [35]. Compositions of the most important Fe-Ti oxide minerals are labeled along with mineral names; titanomagnetite and titanohematite solid solution series are indicated. Both titanomagnetites and titanohematites crystallize at $\sim 1300^\circ\text{C}$, and a solid solution is complete at these high temperatures. Thus, all compositions are possible at high temperatures. On the TiO_2 -FeO- Fe_2O_3 ternary diagram of [36], the chemical analyses of deuteritic oxidation products are plotted along the ulvospinel–magnetite line. Meanwhile, secondary phases are represented by points along the ilmenite–hematite line (Figure 13). The source of the large amount of Fe-Ti oxides in the ferro-gabbros is a product of such primary iron melt enrichment. Fe-Ti oxides most likely originated during high-temperature late/post-magmatic activity.

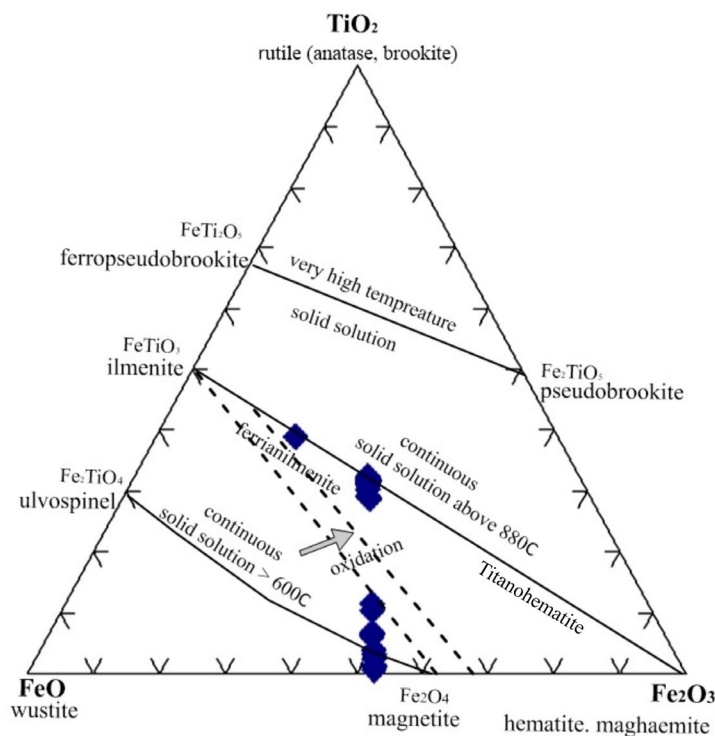


Figure 13. TiO_2 -FeO- Fe_2O_3 solid system diagram showing the composition and approximate equilibrium lines (dashed lines) between analyzed titanomagnetites from gabbro of Abu Ghalaga area [36,37].

The iron content was divided according to the binary relations between FeO and MnO , P_2O_5 , and Al_2O_3 into three groups: low iron content (LIC), which contains FeO ranging from 0 to 11 wt.%, medium iron content (MIC) where FeO ranges from 45 to 51 wt.%, and high iron content (HIC), which contain FeO ranging from 70 to 90 wt.%. The MIC is associated with the mineral ilmenite, while the HIC is mostly related to the mineral magnetite. Magnetite and ilmenite are the most common Fe-Ti oxide ore minerals. Figure 13 shows the overall chemical data, with tie lines illustrating the equilibrium of the oxides in the triangle TiO_2 -FeO- Fe_2O_3 under varying temperature settings. These figures were derived subjectively using typical oxide grain analyses, which included minor exsolution lamellae as much as possible, and will be supplemented by more precise estimates based on the modal analysis of oxide grains. The investigated ilmenite plots on the ferroilmenite

line were generated by continuous solid solution over 800 °C in this diagram, whereas the examined magnetite and Ti–magnetite plot near the magnetite residue at the end of the continuous solid solution above 600 °C.

During the cooling of the intrusions, oxidation caused magnetite to dissolve from the titanomagnetite solid solution, generating either discrete lamellae of magnetite in titanomagnetite or granular ilmenite exsolution surrounding magnetite grains. The formation of ilmenite trellis and lamellae in magnetite and titanomagnetite occurs as a result of an oxidation process [38], which could be caused by (i) an excess of oxygen in titanomagnetite; (ii) trapped oxidizing agents; and (iii) the introduction of an external oxidizing agent. This characteristic could indicate that the parental magma crystallized at high H₂O and oxygen fugacity conditions, as indicated by the modal rise in hydrous minerals. In the crystal structure of ilmenite and magnetite, oxygen atoms are closely packed and stacked cations are layered. The orientations of exsolved magnetite are mostly determined by the dense packing of oxygen atoms [39].

5.2. Genesis of the Abu Ghalaga Ilmenite Ore

Variable genetic models have been proposed for the Fe-Ti oxide deposits associated with mafic and ultramafic rocks. The older models proposed the existence of genetic relationships between the Fe-Ti oxide ores and the host complexes. These mechanisms involve the separation and accumulation of Fe-Ti crystals to form layers, or assume the presence of Fe-Ti oxide liquids from which the ores crystallized [1,40–44]. The fractional crystallization of TiO₂-rich magma led to early ilmenite saturation [45]. Plagioclase buoyant separation was an important step in the production of ilmenite-rich ores [6]. A model for Fe-Ti oxide deposits was proposed based on the density segregation of Fe-Mg silicates and plagioclase, with buoyant plagioclase eliminated to leave a Fe-Ti-rich crystal–liquid mush [46]. The remaining melts may display enrichment in FeO and TiO₂ until Fe-Ti oxide saturation is attained. Liquid immiscibility and fractional crystallization paired with crystal sorting have been proposed as explanations for the high concentration of Fe-Ti oxides. The newer models suggest mechanisms whereby the episodic increase in oxygen fugacity triggers the crystallization of sufficient quantities of Ti-Fe oxides for the development of ore-rich layers [33,47,48].

The origin and evolution of the magma that gave rise to gabbroic rocks in the studied area have been well studied [49]. However, the overall compositions of Fe-Ti oxides and their relationships with magma evolution remain unknown. The Abu Ghalaga deposit is a titaniferous iron ore occurring in a conspicuous gabbroic hill, and the ore and the enclosing gabbro were subjected later to dynamic metamorphism, leading to some alterations in both the gabbro and the ilmenite ore [50]. Therefore, Abu Ghalaga deposits are a late magmatic ore formed by the accumulation of a late ilmenite-rich residual fluid on top of the titaniferous gabbro mass [23]. Khedr et al. [3] claim that the Abu Ghalaga Fe-Ti ores are trending toward tholeiitic ferrobaltic origin along rift settings connected to subduction (Figure 14a). The upwelling asthenosphere or mantle plume that is forcibly injected into the base of the metasomatized lithosphere is a component of the tectonic model of the examined region. Decompression during this injection produced partial melting and the parent melts of SED layered intrusions.

The following crystallization sequence for the ore and the associating gabbroic rocks is (a) an early crystallization stage of the main rock-forming minerals, (b) followed by the crystallization of ilmenite, and (c) terminated in the late stage by the crystallization of sulfides (pyrite), quartz, and potash feldspars. Maurice et al. [23] also suggested that ilmenite was deposited in two stages: a magmatic stage followed later by a metamorphic differentiation stage, to form an ore body possessing the same NW–SE trend as the original gabbro [51].

The Abu Ghalaga ore deposit was produced during the gabbro's magmatic phase (mafic magma). The metamorphic grade that followed was only formed by crystal settling (Figure 14b,c) or filter pressing during the crystallization of the gabbroic magma to form

syngenetic bands in a mafic magma chamber [52–54]. Ilmenite (averaging 67%) is the most abundant mineral in the Abu Ghalaga large ore, with minor amounts of titanomagnetite (4–17%) and hematite (13–18%), and up to 2% sulfides [55,56].

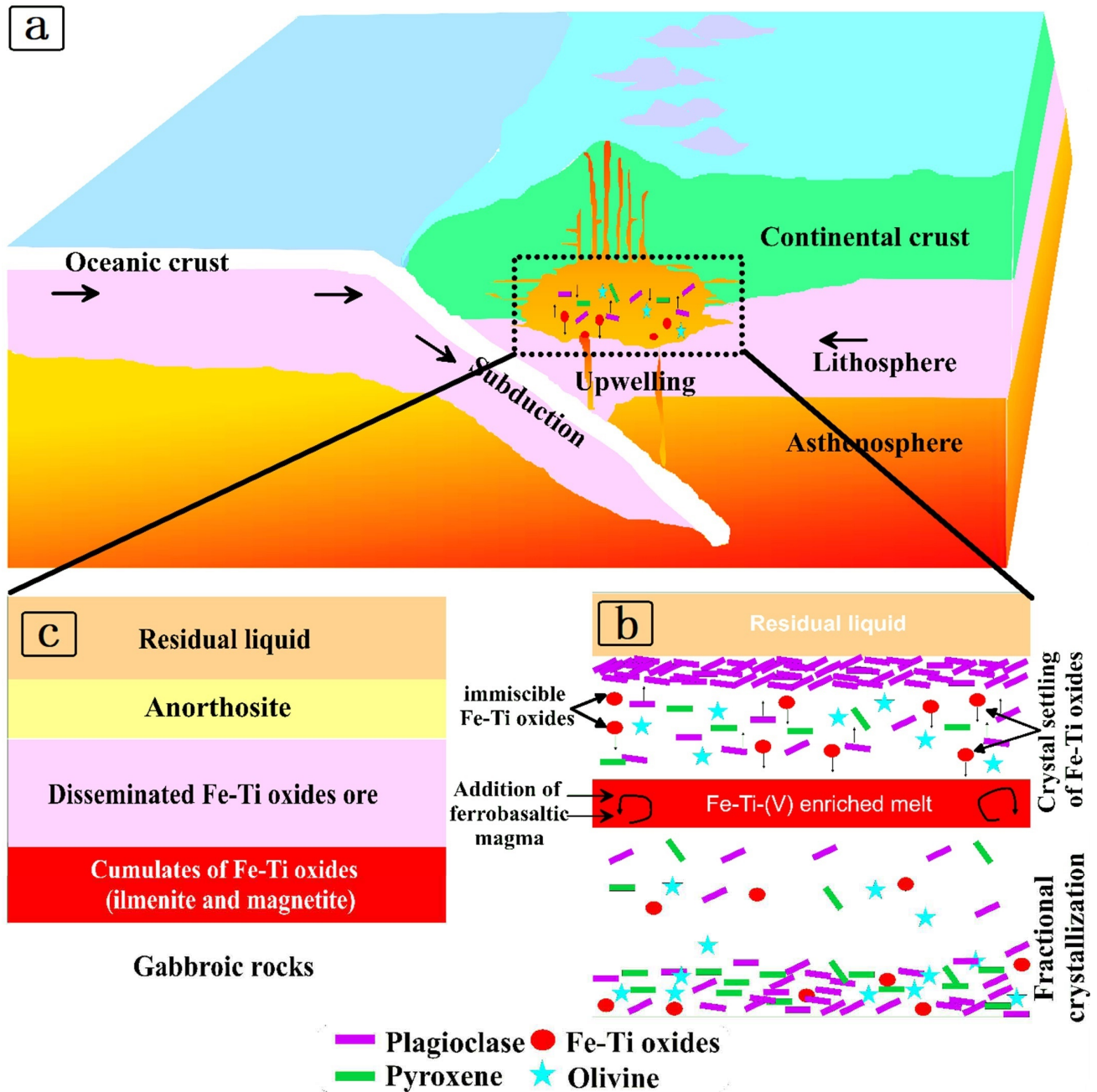


Figure 14. Petrogenetic model for Fe-Ti oxide ores modified after [3,52], accomplished with the Abu Ghalaga intrusion, showing the following: (a) subduction zone showing oceanic crust beneath the continental crust; (b) fractional crystallization of magma accompanied by crystal settling of Fe-Ti oxide crystals; (c) the production of significant Fe-Ti oxide ores caused by the concentration of Fe-Ti oxide crystals following the crystallization of Fe-Ti-(V)-enriched liquids with ferrobasaltic magma.

6. Conclusions

Several Fe-Ti oxide deposits are known in the south-eastern desert of Egypt, in association with mafic-ultramafic masses that include rocks ranging in composition from gabbro-melanorite to anorthosite. The ore mineral assemblages include ilmenite, hematite,

and pyrite, along with gangue minerals, including plagioclase (An₄₀-An₆₀), clinopyroxene, hornblende, tremolite, quartz, zoisite, epidote, and carbonate. Under the scanning electron microscope, ilmenite contains intergrowths of hematite as a thin sandwich and lens shape.

1. XRD analyses confirmed that the SEM and reflected microscopy results were characterized by the presence of ilmenite (Ilm), hematite (Hem), and pyrite (Py).
2. The area of study is affected by the Nugrus shear zone (NW–SE fault; parallel to the Red Sea direction), which represents the southern continuation of the Hafafit shear zone.
3. The ilmenite grains enclose exsolution bodies of hematite lamellae that are segregated within the ilmenite host. Small grains of hematite are exsolved and segregated at the borders of ilmenite grains. Pyrite occurs as independent dissemination in ilmenite samples. The replacement of ilmenite or hematite by pyrite indicates oxidizing conditions. Barium was recorded in the SEM as barite (BaSO₄) and an indicator of highly stable elements in oxidizing (sulfate-stable) environments.
4. Segregation of an immiscible Fe-Ti-rich magma, fractional crystallizations with oxide settling (perhaps accompanied by plagioclase flotation), magma mixing, and solid-state crystallization are some of the major mechanisms responsible for ore formation. Exsolution of magnetite from the titanomagnetite solid solution, shaping either distinct lamellae of magnetite in titanomagnetite or the granular exsolution of ilmenite around grains of magnetite, was created by oxidation during the cooling of the intrusions. The studied samples reveal that the analyzed ilmenite plots on the ferranilmenite line formed by continuous solid solution above 800 °C; meanwhile, the analyzed magnetite and Ti-magnetite plots close to the magnetite lie at the end of the continuous solid solution above 600 °C.
5. According to the binary relations between FeO and MnO, P₂O₅, and Al₂O₃, the iron content was divided into three groups: low iron content (LIC), which contained FeO ranging from 0 to 11 wt.%, medium iron content (MIC) with FeO ranging from 45 to 51 wt.%, and high iron content (HIC) containing FeO ranging from 70 to 90 wt.%.

Author Contributions: Conceptualization, H.M.E.-D.; methodology, H.M.E.-D., A.M.A.-R., W.F., I.K. and S.A.M.; software, H.M.E.-D., A.S. (Adel Shirazy) and A.S. (Aref Shirazi); validation, A.H.; writing—original draft preparation, H.M.E.-D.; writing—review and editing, H.M.E.-D., A.B.P. and A.S. (Aref Shirazi); visualization, H.M.E.-D. All authors have read and agreed to the published version of the manuscript.

Funding: This research received no external funding.

Data Availability Statement: Not applicable.

Acknowledgments: The Geology Department, Faculty of Science, Al-Azhar University, and the Geology Department, Faculty of Science, Suez Canal University, Egyptian Mineral Resources Authority (EMRA), are greatly acknowledged for the laboratory and logistic support. Thanks to the Department of Mining Engineering, Amirkabir University of Technology, Tehran, Iran, and the Institute of Oceanography and Environment (INOS), University Malaysia Terengganu (UMT), for providing facilities during the revision and editing of the manuscript. The anonymous reviewers are acknowledged for their very useful and constructive comments and suggestions for the improvement of this manuscript.

Conflicts of Interest: The authors declare no conflict of interest.

References

1. Lister, G.F. The composition and origin of selected iron-titanium deposits. *Econ. Geol.* **1966**, *61*, 275–310. [[CrossRef](#)]
2. Shirazy, A.; Ziaii, M.; Hezarkhani, A.; Timkin, T. Geostatistical and Remote Sensing Studies to Identify High Metallogenic Potential Regions in the Kivi Area of Iran. *Minerals* **2020**, *10*, 869. [[CrossRef](#)]
3. Khedr, M.Z.; Takazawa, E.; Arai, S.; Stern, R.J.; Morishita, T.; El-Awady, A. Styles of Fe–Ti–V ore deposits in the Neoproterozoic layered mafic-ultramafic intrusions, south Eastern Desert of Egypt: Evidence for fractional crystallization of V-rich melts. *J. Afr. Earth Sci.* **2022**, *194*, 104620. [[CrossRef](#)]

4. Gross, G.A. Algoma-type iron-formation. *Sel. Br. Columbia Miner. Depos. Profiles* **1996**, *2*, 1–13.
5. Shirazy, A.; Hezarkhani, A.; Timkin, T.; Shirazi, A. Investigation of Magneto-/Radio-Metric Behavior in Order to Identify an Estimator Model Using K-Means Clustering and Artificial Neural Network (ANN) (Iron Ore Deposit, Yazd, IRAN). *Minerals* **2021**, *11*, 1304. [[CrossRef](#)]
6. Charlier, B.; Skar, O.; Korneliussen, A.; Duchesne, J.C.; Vander Auwera, J. Ilmenite composition in the Tellnes Fe-Ti deposit, SW Norway: Fractional crystallization, post cumulus evolution and ilmenite-zircon relation. *Contrib. Mineral. Petrol.* **2007**, *154*, 119–134. [[CrossRef](#)]
7. El Khallofi, M.; Drevelle, O.; Soucy, G. Titanium: An overview of resources and production methods. *Minerals* **2021**, *11*, 1425. [[CrossRef](#)]
8. Towner, R.R.; Gray, J.M.; Porter, L.M. *International Strategic Minerals Inventory Summary Report, Titanium*; US Geological Survey: Reston, VA, USA, 1988.
9. Force, E.R. Titanium content and titanium partitioning in rocks. In *Geology and Resources of Titanium*; U.S. Government Printing Office: Washington, DC, USA, 1976; pp. A2–A3.
10. Abu El-Rus, M.A. Geological studies on Abu Ghalaga area, Eastern Desert, Egypt. Master's Thesis, Assiut University, Assiut, Egypt, 1991; 255p.
11. Greiling, R.O.; Abdeen, M.M.; Dardir, A.A.; El-Akhal, H.; El-Ramly, M.F.; Kamal El-Din, G.M.; Osman, A.F.; Rashwan, A.A.; Rice, A.H.; Sadek, M.F. A structural synthesis of the Proterozoic Arabian-Nubian Shield in Egypt. *Geol. Rundsch.* **1994**, *83*, 484–501. [[CrossRef](#)]
12. Hassan, S.M.; El-Kazzaz, Y.A.; Taha, M.N.; Mohammad, A.T. Late Neoproterozoic basement rocks of Meatiq area, Central Eastern Desert, Egypt: Petrography and remote sensing characterizations. *J. Afr. Earth Sci.* **2017**, *131*, 14–31. [[CrossRef](#)]
13. El-Kalioubi, B.; Fowler, A.; Abdelmalik, K. Chapter 6: The Metamorphism and Deformation of the Basement Complex in Egypt. In *Geology of Egypt*; Springer: Berlin/Heidelberg, Germany, 2020; pp. 191–252. [[CrossRef](#)]
14. El-Desoky, H.M.; Tende, A.W.; Abdel-Rahman, A.M.; Ene, A.; Awad, H.A.; Fahmy, W.; El-Awny, H.; Zakaly, H.M. Hydrothermal alteration mapping using landsat 8 and ASTER data and geochemical characteristics of Precambrian rocks in the Egyptian shield: A Case Study from Abu Ghalaga, Southeastern Desert, Egypt. *Remote Sens.* **2022**, *14*, 3456. [[CrossRef](#)]
15. Nasr, B.B.; Sadek, M.F.; Masoud, M.S. Some new occurrences of layered titanomagnetite. Eastern Desert, Egypt. *Ann. Geol. Surv. Egypt* **2008**, *23*, 679–690.
16. Makhlof, A.; Beniamin, N.Y.; Mansour, M.M.; Mansour, S.A.; El-Shrbeni, H. Mafic-ultramafic intrusion of South Korab Kansi area with emphasis on titanomagnetite ores, southern Eastern Desert, Egypt. *Ann. Geol. Surv. Egypt* **2008**, *3*, 1–20.
17. Saleh, G.M.; Khaleal, F.M.; Lasheen, E.S.R. Petrogenesis of ilmenite-bearing mafic intrusions: A case study of Abu Ghalaga area, South Eastern Desert, Egypt. *Arab. J. Geosci.* **2022**, *15*, 1508. [[CrossRef](#)]
18. Mikulski, S.Z.; Sadłowska, K.; Wiszniewska, J.; Małek, R. Vanadium and Cobalt Occurrence in the Fe-Ti-V Oxide Deposits Related to Mesoproterozoic AMCG Complex in NE Poland. *Appl. Sci.* **2022**, *12*, 6277. [[CrossRef](#)]
19. Fritz, H.; Wallbrecher, E.; Khudeir, A.A.; Abu-El Ela, F.; Dallmeyer, D.R. Formation of Neoproterozoic core complexes during oblique convergence (Eastern Desert, Egypt). *J. Afr. Earth Sci.* **1996**, *23*, 311–329. [[CrossRef](#)]
20. Abd El-Wahed, M.A. Oppositely dipping thrusts and transpressional imbricate zone in the Central Eastern Desert of Egypt. *J. Afr. Earth Sci.* **2014**, *100*, 42–59. [[CrossRef](#)]
21. Abdel Aziz, Y.M. Manganian Ilmenite from the gabbroic rocks of Abu Ghalaga area, Eastern Desert, Egypt. In Proceedings of the 2nd International Conference on the Geology of Africa, Assiut, Egypt, October; 2001; Volume 1, pp. 101–121.
22. Maurice, A.E.; Basta, F.F.; Khiamy, A.A. Neoproterozoic nascent island arc volcanism from the Nubian Shield of Egypt: Magma genesis and generation of continental crust in intra-oceanic arcs. *Lithos* **2012**, *132–133*, 1–20. [[CrossRef](#)]
23. Amin, M.S. The ilmenite deposit of Abu Ghalaga. *Econ. Geol.* **1954**, *49*, 77–87. [[CrossRef](#)]
24. Abdel-Karim, A.A.M.; Elwan, W.I.; Helmy, H.; El-Shafey, S.A. Spinels, Fe–Ti oxide minerals, apatites, and carbonates hosted in the ophiolites of Eastern Desert of Egypt: Mineralogy and chemical aspects. *Arab. J. Geosci.* **2014**, *7*, 693–709. [[CrossRef](#)]
25. Deer, W.A.; Howie, R.A.; Zussman, J. *An Introduction to the Rock Forming Minerals*; Longman: London, UK, 1992; p. 696.
26. Mehdilo, A.; Irannajad, M. Effects of mineralogical and textural characteristics of ilmenite; concentrate on synthetic rutile production. *Arab. J. Geosci.* **2013**, *6*, 3865–3876. [[CrossRef](#)]
27. Du, Y.; Meng, Q.; Yuan, Z.; Ma, L.; Zhao, X.; Xu, Y. Study on the flotation behavior and mechanism of ilmenite and titanite with sodium oleate. *Miner. Eng.* **2020**, *152*, 106366. [[CrossRef](#)]
28. Whitney, D.L.; Evans, B.W. Abbreviations for names of rock-forming minerals. *Am. Mineral.* **2010**, *95*, 185–187. [[CrossRef](#)]
29. Haggerty, S.E. Opaque Mineral Oxides in Terrestrial Igneous Rocks. In *Oxide Minerals*; Reviews in Mineralogy and Geochemistry; Rumble, D., Ed.; Mineralogical Society of America: Chantilly, VA, USA, 1976; Volume 3, pp. Hg101–Hg300.
30. Dunlop, D.; Ozdemir, O. *Fundamental Frontiers*; Cambridge Studies in Magnetism; Cambridge University Press: New York, NY, USA, 1997; 573p.
31. Bai, Z.J.; Zhong, H.; Naldrett, A.J.; Zhu, W.G.; Xu, G.W. Whole-rock and mineral composition of constraints on the genesis of the giant Hongge Fe–Ti–V oxide deposit in the Emeishan LIP, southwest China. *Econ. Geol.* **2012**, *107*, 481–506. [[CrossRef](#)]
32. Pang, K.N.; Zhou, M.F.; Lindsley, D.; Zhao, D.; Malpas, J. Origin of Fe–Ti oxide ores in mafic intrusions: Evidence from the Panzhihua intrusion, SW China. *J. Petrol.* **2008**, *49*, 295–313. [[CrossRef](#)]

33. Zhou, M.F.; Chen, W.T.; Wang, C.Y.; Prevec, S.A.; Liu, P.P.; Howarth, G. Two stages of immiscible liquid separation in the formation of Panzhihua-type of Fe–Ti–V oxide deposits, SW China. *Geosci. Front.* **2013**, *4*, 481–502. [[CrossRef](#)]
34. Charlier, B.; Grove, T.L. Experiments on liquid immiscibility along tholeiitic liquid lines of descent. *Contrib. Mineral. Petrol.* **2012**, *164*, 27–44. [[CrossRef](#)]
35. Withers, P.J.; Ulen, B.; Stamm, C.; Bechmann, M. Incidental phosphorus losses—Are they significant and can they be predicted. *J. Plant Nutr. Soil Sci.* **2003**, *166*, 459–468. [[CrossRef](#)]
36. Broska, I.; Uher, P.; Ondrejka, M. *Geochemical and Mineralogical Characterization of the Fe-Ti Oxide Paragenesis in the Magmatic and Hydrothermal Systems of the Western Carpathians*; Slovak Academy of Sciences: Bratislava, Slovakia, 2003. Available online: <http://www.geol.sav.sk/broska/projects.html> (accessed on 23 August 2022).
37. Buddington, A.F.; Lindsley, D.H. Iron-titanium oxide minerals and synthetic equivalent. *J. Petrol.* **1964**, *5*, 310–357. [[CrossRef](#)]
38. Al-Mohandis, A.A. The opaque minerals of Jabal Sha layered intrusion, Saudi Arabia. *J. Coll. Sci. Riyadh* **1980**, *11*, 171–188.
39. Wenk, H.R.; Chen, K.; Smith, R. Morphology and microstructure of magnetite and ilmenite inclusions in plagioclase from Adirondack anorthositic gneiss. *Am. Mineral.* **2011**, *96*, 1316–1324. [[CrossRef](#)]
40. Hall, A.L. *The Bushveld Igneous complex of the Central Transvaal*; Memoir No. 28; Geological Survey of the Union of South Africa: Pretoria, South Africa, 1932.
41. Bateman, A.M. The formation of late magmatic oxide ores. *Econ. Geol.* **1951**, *46*, 404–426. [[CrossRef](#)]
42. Kolker, A. Mineralogy and geochemistry of Fe-Ti oxide and apatite (nelsonite) deposits and evaluation of liquid immiscibility hypothesis. *Econ. Geol.* **1982**, *77*, 1146–1158.
43. Philpotts, A.R. Origin of certain iron-titanium oxide and apatite rocks. *Econ. Geol.* **1967**, *62*, 303–315. [[CrossRef](#)]
44. Reynolds, I.M. The nature and origin of titaniferous magnetite-rich layers on the upper zone of the Bushveld complex: A review and synthesis. *Econ. Geol.* **1985**, *80*, 1089–1108. [[CrossRef](#)]
45. Charlier, B.; Duchesne, J.C.; Vander Auwera, J. Magma chamber processes in the Tellnes ilmenite deposit (Rogaland Anorthosite Province, SW Norway) and the formation of Fe-Ti ores in massif-type anorthosites. *Chem. Geol.* **2006**, *234*, 264–290. [[CrossRef](#)]
46. Woodruff, L.G.; Nicholson, S.W.; Fey, D.L. A deposit model for magmatic iron-titanium oxide deposits related to Proterozoic massif anorthosite plutonic suites. *U.S. Geol. Surv. Sci. Investig. Rep.* **2013**, *5091*, 47.
47. Zhou, M.F.; Robinson, P.T.; Leshner, C.M.; Keays, R.R.; Zhang, C.J.; Malpas, J. Geochemistry, petrogenesis and metallogenesis of the Panzhihua gabbroic layered intrusion and associated Fe-Ti-V oxide deposits, Sichuan Province, SW China. *J. Petrol.* **2005**, *46*, 22–53. [[CrossRef](#)]
48. Hou, T.; Zheng, Z.; Encarnacion, J.; Santosh, M. Petrogenesis and metallogenesis of the Taihe gabbroic intrusion associated with Fe-Ti oxide ores in the Panxi district, Emeishan large igneous province. *Ore Geol. Rev.* **2012**, *49*, 109–127. [[CrossRef](#)]
49. El-Metwally, A.A. Petrogenesis of gabbroic rock intrusions from south-central Sinai massif: A transition from arc to intraplate magmatism. In Proceedings of the Third International Conference on Geochemistry, Alexandria, Egypt, 5–6 June 2015; pp. 49–66.
50. Attia, M.I. *The Geology of the Iron-Ore Deposits*; Geological Survey: Cairo, Egypt, 1950.
51. El-Shazly, E.M. *The Ilmenite Ore at Abu Ghalaga, Eastern Desert, Egypt*; Report 3759; Geological Survey: Cairo, Egypt, 1959.
52. Cao, J.; Wang, X.; Tao, J. Petrogenesis of the Piqiang mafic-ultramafic layered intrusion and associated Fe-Ti-V oxide deposit in Tarim Large Igneous Province, NW China. *Int. Geol. Rev.* **2019**, *61*, 2249–2275. [[CrossRef](#)]
53. Basta, E.Z.; Takla, M.A. Petrological Studies on Abu Ghalaga Ilmenite Occurrence, Eastern Desert. *Egypt J. Geol.* **1968**, *12*, 43–71.
54. Hussein, A.A. Mineral deposits. In *The Geology of Egypt*; Said, R., Ed.; Routledge: Abingdon, UK, 2001; pp. 537–539.
55. Shirazi, A.; Hezarkhani, A.; Beiranvand Pour, A.; Shirazy, A.; Hashim, M. Neuro-Fuzzy-AHP (NFAHP) Technique for Copper Exploration Using Advanced Spaceborne Thermal Emission and Reflection Radiometer (ASTER) and Geological Datasets in the Sahlabad Mining Area, East Iran. *Remote Sens.* **2022**, *14*, 5562. [[CrossRef](#)]
56. Hawa, Y.M.A. Mineral chemistry of extraordinary ilmenite from the Gabbroic rocks of Abu Ghalaga area, Eastern Desert, Egypt: Evidence to metamorphic modification. In Proceedings of the 6th International Conference on Geological Sciences and Engineering (ICGSE), Paris, France, 28–29 August 2014; Volume 1, p. 68, (Abstract). Available online: www.waset.org/abstracts/7253 (accessed on 6 August 2020).

Disclaimer/Publisher’s Note: The statements, opinions and data contained in all publications are solely those of the individual author(s) and contributor(s) and not of MDPI and/or the editor(s). MDPI and/or the editor(s) disclaim responsibility for any injury to people or property resulting from any ideas, methods, instructions or products referred to in the content.